Inorganic Sulfur Species formed upon Heterogeneous OH Oxidation of Organosulfates: A Case Study of Methyl Sulfate

Rongshuang Xu,[a] Yao Ge,[b] Kai Chung Kwong,[a] Hon Yin Poon,[a] Kevin R. Wilson,[c] Jian Zhen Yu[b] and Man Nin Chan[a,d,]*

[a] Earth System Science Programme, Faculty of Science, The Chinese University of Hong Kong, Hong Kong, China

[b] Department of Chemistry, The Hong Kong University of Science and Technology, Hong Kong, China

[c] Chemical Sciences Division, Lawrence Berkeley National Laboratory, Berkeley, CA, USA

[d] The Institute of Environment, Energy, and Sustainability, The Chinese University of Hong Kong, Hong Kong, China

* Corresponding author: Man Nin Chan, Email: mnchan@cuhk.edu.hk

Abstract. Recent studies reveal that organosulfates at the particle surface can be oxidized by gas-phase OH radicals with significant rates. Inorganic sulfur species, such as the bisulfate ion (HSO_4^-) and sulfate ion (SO_4^{2-}), can be formed upon these heterogeneous oxidation processes through the formation and subsequent reactions of sulfate radical anion ($SO_4^{\bullet-}$) in the particle phase. However, the amount of inorganic sulfur species produced in these heterogeneous oxidation reactions is not known. We investigate the heterogeneous OH oxidation of sodium methyl sulfate (CH_3SO_4Na), the smallest organosulfate detected in atmospheric particles, using an oxidation flow reactor at a relative humidity of 75 %. We quantify the kinetics by measuring the decay of CH_3SO_4Na and the amount of HSO_4^- and SO_4^{2-} formed upon oxidation using ion chromatography. Kinetic measurements determine the heterogeneous OH reaction rate to be $(5.72 \pm 0.14) \times 10^{-13}$ cm^3 molecule^{-1} s^{-1}, with an effective OH uptake coefficient, γ_{eff}, of 0.31 ± 0.06. The molar yield of inorganic sulfur species, defined as the total number of moles of HSO_4^- and SO_4^{2-} formed per mole of CH_3SO_4Na consumed upon oxidation, is found to be significant and has an average value of 0.62 ± 0.18 upon oxidation. A kinetic model is developed to describe the kinetics and inorganic sulfur species formation upon oxidation. Model simulations suggest that CH_3SO_4Na tends to decompose rapidly into formaldehyde and $SO_4^{\bullet-}$, and the reaction of $SO_4^{\bullet-}$ with CH_3SO_4Na plays a significant role in both governing the kinetics and the formation of inorganic sulfur species.

Keywords: Heterogeneous oxidation, organosulfates, inorganic sulfates, particle sulfur chemistry, sulfate radical reactions

INTRODUCTION

Increasing evidence has revealed that sulfur in atmospheric particles can exist in its organic form, namely, organosulfur compounds. By determining the difference between total sulfur and inorganic sulfur measured by X-ray fluorescence (XRF) and ion chromatography (IC) respectively, organosulfur compounds can contribute up to 30 % of total organic particle mass at a forest site in K-puszta, Hungary.[1] Using the same approach with the National Park Service IMPROVE $PM_{2.5}$ database, Tolocka and Turpin reported that organosulfur compounds can account for 5−10 % of total organic particle mass across different regions in the United States.[2] Generally, the amount of organosulfur compounds depends on the season and location and appears to be higher with elevated photochemical activity.

Organosulfates are characterized by the sulfate ester functional group ($R-O-SO_3^-$) and are one of the most important classes of organosulfur compounds detected in atmospheric particles.[3] The formation mechanisms of organosulfates have been investigated in many studies and summarized elsewhere.[1, 3-21] Once formed, organosulfates are expected to continuously transform in the atmosphere. Some organosulfates (e.g. tertiary organosulfates) can undergo hydrolysis at efficient rates to form polyols and sulfuric acid with a time scale of a few to tens of hours under typical atmospheric conditions. For instance, the lifetime for hydrolysis of 2-methyl-2-sulfato-1-propanol is only about 2.5 hours.[22] More recently, we found that the sodium salt of methyl sulfate (CH_3SO_4Na), the smallest organosulfate found in atmospheric particles, can be oxidized efficiently by gas-phase OH radicals at or near the particle surface.[23] Such heterogeneous oxidative process can proceed with an effective OH uptake coefficient, γ_{eff}, of 0.17 ± 0.03 and an atmospheric lifetime of ~ 20 days at relative humidity (RH) of 85 %. A single major product peak of bisulfate ion (HSO_4^-) has been detected in the particle mass spectra using a soft ambient

pressure ionization source (Direct Analysis in Real Time, DART) coupled with a high-resolution mass spectrometer.[23] These results suggest that a portion of particle sulfur was being converted from its organic form to its inorganic form upon oxidation. However, the amount of inorganic sulfur species formed upon oxidation cannot be quantified by the DART technique and remains unknown. Given the sulfur in its inorganic and organic form exhibit different physiochemical properties (e.g. surface activity, water uptake and cloud condensation nuclei activity),[24-26] it would be desirable to understand the chemical interconversion between the inorganic and organic sulfur species.

In this work, we extend our previous work on the heterogenous OH oxidation of CH_3SO_4Na[23] and focus on investigating the amount of inorganic sulfur species formed upon heterogeneous OH oxidation using an oxidation flow reactor (OFR) at 298 K and 75 % RH (Table 1). Particles leaving the reactor were collected on Teflon filters before and after OH oxidation for subsequent chemical analysis. The amount of methyl sulfate ($CH_3SO_4^-$) and sulfate (SO_4^{2-}) ions were quantified using ion chromatography (IC). We would like to acknowledge that as shown in reaction mechanisms (Scheme 1), both HSO_4^- and SO_4^{2-} can be formed upon heterogeneous OH oxidation of CH_3SO_4Na. HSO_4^- is known to be converted into SO_4^{2-} upon injection into IC and mixing with an alkaline mobile phase solution. Hence, the amount of SO_4^{2-} quantified by the IC method would represent the total amount of HSO_4^- and SO_4^{2-} produced upon oxidation. In the following, we first quantify the oxidative kinetics by measuring the decay of CH_3SO_4Na at different extents of OH oxidation. Second, the molar yield of inorganic sulfur species, defined as the total number of moles of HSO_4^- and SO_4^{2-} formed per mole of CH_3SO_4Na reacted, is determined at different extents of oxidation. Lastly, a kinetic model is developed to predict the kinetics and the formation of inorganic sulfur species formed upon oxidation. Model simulations

were also performed to examine how the change in RH would alter the heterogenous reactivity. Overall, the results of this work would provide new insights into the conversion of sulfur between its organic and inorganic forms during heterogenous OH oxidation of CH_3SO_4Na particles.

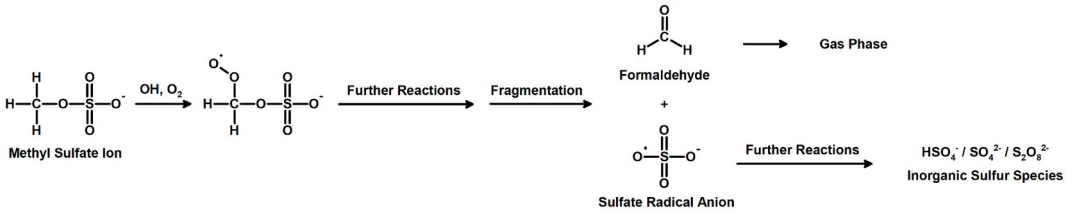

Scheme 1. Simplified reaction pathways proposed for the heterogeneous OH oxidation of sodium methyl sulfate.[23]

Table 1. Experimental conditions and reaction kinetics, and molar yield of inorganic sulfur species (HSO_4^- and SO_4^{2-}) during heterogeneous OH oxidation.

Compounds	Sodium Methyl Sulfate	
Chemical Structure	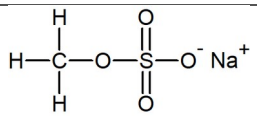	
Molecular Formula	CH_3SO_4Na	
Molecular Weight (g mol^{-1})	134.0867	
Experiments		
Relative Humidity (RH %)	75	85 [a]
Analytical Method	IC	DART
OH Exposure ($\times 10^{11}$ molecules cm^{-3} s)	2.0 ± 0.4–19.0 ± 3.8	1.2 ± 0.3–12.7 ± 2.5
Initial particle diameter (nm)	204	218
Mass Fraction of CH_3SO_4Na	0.46	0.34
Effective Heterogeneous OH Oxidation Rate Constant, *k*	5.72 ± 0.14	3.79 ± 0.19

($\times 10^{-13}$ cm^3 molecule^{-1} s^{-1})		
Effective OH Uptake Coefficient, γ_{eff}	0.31 ± 0.06	0.17 ± 0.03
Molar yield of inorganic sulfur species [b]	0.62 ± 0.18	Not measured

[a] Data have been reported in our previous study.[23]
[b] Averaged molar yield of inorganic sulfur species (HSO_4^- and SO_4^{2-}) quantified by IC.

METHODS

Heterogenous OH Oxidation of Sodium Methyl Sulfate Particles

The heterogeneous OH oxidation of CH_3SO_4Na particles was investigated using an OFR with a volume of approximately 13 L (18-inch length, 8-inch inner diameter) at 75 % RH and 298K (Figure 1). The experimental setup and procedures had been described elsewhere.[27–30] In brief, aqueous CH_3SO_4Na particles were first generated by passing its solution through a constant output atomizer (TSI Model 3076). Before entering the reactor, the particles were mixed with nitrogen (N_2), oxygen (O_2) and ozone (O_3) to make up a total flow of ~ 5 L min^{-1}, corresponding to a residence time of ~ 156 s. The humidity inside the reactor was maintained by varying the mixing ratio of dry and humidified N_2. The RH and temperature of the flow exiting the reactor were measured by a RH-temperature sensor (Vaisala, HM40).

Inside the reactor, OH was generated via photolysis of O_3 in the presence of water vapor. The O_3 was generated by passing O_2 through an O_3 generator (ENALY 1000BT-12). The O_3 concentration in the reactor, monitored by an O_3 analyzer (2B technologies, Model 202), ranged from 0 to 12.4 ppm, corresponding to a maximum OH exposure of 19.0×10^{11} molecules cm^{-3} s. The OH exposure, which is equivalent to the product of gas-phase OH concentration and residence time, was determined by measuring the decay of sulfur dioxide (SO_2) in independent experiments (Teledyne SO_2 analyzer, Model T100), following the procedures as described previously.[28, 29] Furthermore, SO_2 calibration experiments in the presence of CH_3SO_4Na particles

were conducted to investigate the effects of the particles on the generation and concentration of gas-phase OH radicals inside the reactor. A variation of ~10 % in the determination of OH exposure was observed over the experimental conditions. The particle stream exiting the reactor then passed through an annular Carulite® catalyst denuder and an activated charcoal denuder for the removal of O_3 and gas-phase species remaining in the stream, respectively. Therefore, only particle-phase reaction products were analyzed. Size distribution of the particles was measured with a scanning mobility particle sizer (SMPS, TSI). Particles leaving the reactor were collected by Teflon filters (2.0 μm pore size, Pall Corporation) at a sampling flow rate of 3 L min^{-1} for 30 minutes. A total volume of 90 L was sampled at a given extent of oxidation. It acknowledges that our previous study has shown that CH_3SO_4Na does not react with O_3 and undergoes photolysis.[23] Furthermore, the OFR was specifically designed with a small surface-to-volume ratio to minimize the particle wall loss.[27-29] The particle transmission efficiency for particle diameter larger than 150 nm was greater than 80 %.[27-29] The wall loss of particles was expected to be small, as the particle diameter was 204 nm and the particles with diameter larger than 150 nm accounted for a significant fraction of total particle mass.[30]

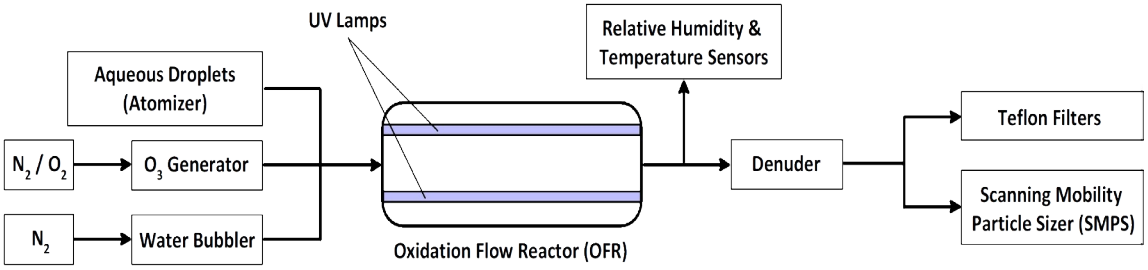

Figure 1. Experimental setup for the heterogeneous OH oxidation of sodium methyl sulfate particles.

Chemical Analysis

The amount of methyl sulfate ($CH_3SO_4^-$) and sulfate (SO_4^{2-}) ions at different extent of oxidation were quantified using IC. The experimental details have been given elsewhere.[31] Briefly, each filter was extracted using 4 mL of double de-ionized water (18.2 MΩ cm) from the ultrapure water system (Nanopure Diamond UV/UF). All samples were sonicated for 60 minutes and then mechanically shaken for 60 minutes. The extract was subsequently analyzed by an ion chromatograph (Dionex ICS-1100). The separation of anions ($CH_3SO_4^-$ and SO_4^{2-}) was accomplished using an AS11-HC analytical column (IonPac, 4 × 250 mm) and an AG11-HC guard column (IonPac, 4 × 50 mm) with 20 mmol L^{-1} NaOH as the eluent. Sodium bisulfate ($NaHSO_4$) and sodium sulfate (Na_2SO_4) standards were used for quantifying inorganic sulfur species. As shown in Figure S1 (Supporting information (SI)), $CH_3SO_4^-$ and SO_4^{2-} can be reasonably separated. The retention times of $CH_3SO_4^-$ and SO_4^{2-} peak are 4.87 and 5.28 minutes, respectively. HSO_4^- is converted into SO_4^{2-} upon mixing with the alkaline eluent. Thus, the peak from injection of the $NaHSO_4$ standard has the same retention time as that from injection of the Na_2SO_4 standard. We note that a small peak exists in the chromatogram of CH_3SO_4Na standard which has a retention time resembling that of SO_4^{2-}. This suggests that a small amount of CH_3SO_4Na (~ 3–4 %) has been converted into SO_4^{2-} during the analysis. This has been corrected when quantifying the amount of SO_4^{2-} formed upon oxidation. As shown in Figure S2 (SI), the responses of the $NaHSO_4$ and Na_2SO_4 standards are approximately the same, suggesting that the choice between $NaHSO_4$ and Na_2SO_4 standards would not have an effect on the quantification of HSO_4^- and SO_4^{2-}. In this work, $NaHSO_4$ was chosen for quantification purpose and the amount of SO_4^{2-} quantified by the IC method would represent the total amount of HSO_4^- and SO_4^{2-} produced upon oxidation. The experimental uncertainty for the measurement of $CH_3SO_4^-$ and SO_4^{2-} is discussed in SI.

Kinetic Model

A kinetic model was developed using the Kinetiscope (http://hinsberg.net/kinetiscope/), which applies stochastic algorithms for kinetic simulation. The particle is modelled as a rectangular compartment [32] with 1×1×R/3 nm^3 volume where R is the initial particle diameter.[33-34] At high RH (75 % RH), CH_3SO_4Na particles are aqueous droplets based on hygroscopic data reported in the literature.[24] It is likely that the species diffuse rapidly within the particles. All species are thus assumed to be well mixed within the particle. For the simulation of heterogeneous reaction, gas-phase OH radicals first adsorb onto the particle surface. The pseudo-first order adsorption rate constant for gas-phase OH radicals on the particle surface is determined below:[35]

$$k_{ads} = [OH] \times S \times Z \quad (1)$$

where S is the sticking coefficient, and Z is the collision frequency between gas-phase OH radical and particle surface, given by σ×ν, with σ as collision cross-section (1×1 nm^2), and ν is the mean speed of gas-phase OH radical. As proposed previously,[36] the adsorption of gas-phase OH radicals generally occurs in the top compartment. One nm is chosen to be the thickness of the accessible region on the particle surface for oxidation.

Scheme 1 shows the OH radical reacts with CH_3SO_4Na by abstracting a hydrogen atom, forming an alkyl radical, which quickly reacts with an oxygen molecule to form a peroxy radical. Alkoxy radicals resulted from the self-reactions of two peroxy radicals decompose to formaldehyde and sulfate radical anions ($SO_4^{\bullet-}$). Formaldehyde tends to partition back to the gas phase due to its high volatility. The evaporation rate constant, k_{evap}, was calculated by the following equation:[37]

$$k_{evap} = \frac{V_¿ 6\, p_{sat} \sqrt{N_A}}{A_¿ [CH_3SO_4Na]_0 2\pi M\, k_B T} \quad (2)$$

where $V_¿$ is the simulated particle volume (nm^3), defined by 1 nm x 1 nm x R/3 nm rectangular volume. $A_¿$ is the simulated area (1 nm × 1 nm), $[CH_3SO_4Na]_0$ is the initial CH_3SO_4Na concentration (molecules cm^{-3}), N_A is the Avogadro constant (mol^{-1}), M is the molar mass of CH_3SO_4Na ($g \cdot mol^{-1}$), k_B is the Boltzmann constant ($m^2 \cdot kg \cdot s^{-2} \cdot K^{-1}$), T is the temperature (K), and p_{sat} is the saturation vapor pressure ($kg \cdot m^{-1} \cdot s^{-2}$). Unlike formaldehyde, $SO_4^{\bullet -}$ remains in the particle phase and undergoes further reactions which can possibly form various inorganic sulfur species, such as HSO_4^-, SO_4^{2-} and peroxydisulfate ($S_2O_8^{2-}$) ions.

Reaction schemes and rate constants used in the model are obtained from literatures with justifications and are given in Table 2. We note that the knowledge of rate constants for the reactions involving organosulfates and their radicals is very limited. It is not yet possible, or at least difficult, to describe the rate of the reactions (e.g. rate coefficients and sticking coefficient) very accurately. Although the modelled results show a good agreement with the experimental observations, rate constants used in the model (Table 2) should be used with caution and are required to be further tested with experimental data. Since the model which includes an explicit description of the reactions can be used to study the influence of individual reaction or combinations of reactions on the kinetics and the formation of inorganic sulfur species upon oxidation, this work includes sensitivity tests on rate constants to evaluate the performance of the model towards the reactions.

Table 2. Reaction schemes and rate constants for the kinetic model at 298 K.

No.	Reaction	Rate constant	Remark
	site $\overset{k_{ads}}{\rightarrow}$ $\bullet OH_{ads}$	$k_{ads} = [OH] \times S \times Z$	Houle and co-workers[36,a]
R1	$RH + \bullet OH_{ads} \rightarrow R\bullet + H_2O$	$k_1 = 5.81 \times 10^{-13}$	Monod and Doussin[38,b]

		cm^3 $molecule^{-1}$ s^{-1} (= 3.50×10^8 L mol^{-1} s^{-1})	
R2	$R\bullet + O_2 \rightarrow ROO\bullet$	$k_2 = 1.13 \times 10^6$ s^{-1}	Marchaj and co-workers [39,c]
R3	$2ROO\bullet \rightarrow 2RO\bullet$	$k_3 = 6.64 \times 10^{-13}$ cm^3 $molecule^{-1}$ s^{-1} (= 4.00×10^8 L mol^{-1} s^{-1})	Nikolaev and co-workers[40,d]
R4	$RO\bullet \rightarrow HCHO_{(aq)} + SO_4^{\bullet-}$	$k_4 = 1.50 \times 10^4$ s^{-1}	Vereecken and Peeters[41,e]
R5	$HCHO_{(aq)} \rightarrow HCHO_{(g)}$	$k_5 = 1.88 \times 10^{15}$ s^{-1}	Heine and co-workers[35]
R6	$SO_4^{\bullet-} + RH \rightarrow HSO_4^- + R\bullet$	$k_6 = 1.10 \times 10^{-17}$ cm^3 $molecule^{-1}$ s^{-1} (= 6.62×10^3 L mol^{-1} s^{-1})	Huie and Clifton[42,f]
R7	$SO_4^{\bullet-} + SO_4^{\bullet-} \rightarrow S_2O_8^{2-}$	$k_7 = 1.26 \times 10^{-12}$ cm^3 $molecule^{-1}$ s^{-1} (= 7.60×10^8 L mol^{-1} s^{-1})	Jiang and co-workers[43]
R8	$SO_4^{\bullet-} + H_2O \rightarrow HSO_4^- + \bullet OH$	$k_8 = 300$ s^{-1}	Hayon and co-workers[44,g]
R9	$HSO_4^- \Leftrightarrow SO_4^{2-} + H^+$	$K_a = 1.20 \times 10^{-2}$	Smith and Martell[45,h]

[a] k_{ads} refers to a pseudo-first order OH adsorption rate constant and has a unit of s^{-1} at a given gas-phase OH radical concentration. Site is an adsorption site on the surface (the top 1 nm thick compartment), which was determined by multiplying the number of initial CH_3SO_4Na density with the number of sites per molecule (assuming 1 site per molecule). The sticking coefficient, S has been reported to be in the order of 10^{-2} to 10^{-3} for different unreactive substrates.[46] A value of 9.5×10^{-3} is used in the model.

[b] This value refers to hydrogen abstraction rate from -CH_3 group by OH radical in aqueous phase estimated using an aqueous-phase structure–activity relationship model.[38]

[c] This value is treated as a pseudo first-order rate constant which has considered the reaction between methyl radical ($CH_3\bullet$) and O_2 (k = 6.81×10^{-12} cm^3 $molecule^{-1}$ s^{-1} (= 4.10×10^9 L mol^{-1} s^{-1}))[39], the gas-phase O_2 concentration of 21 % and the dimensionless Henry's law constant for O_2 (3.18×10^{-2}).

[d] This value refers to the self-reaction rate of methylperoxy radicals in aqueous phase.[40] The ROO• self-reaction which can potentially form a carbonyl-alcohol pair is not considered since no functionalization products have been detected upon heterogeneous OH oxidation of CH_3SO_4Na.[23]

[e] This value refers to a first-order rate constant for $CH_3CH(O\bullet)(ONO_2) = CH_3CHO + \bullet ONO_2$, determined by the structure–activity relationship model developed for the decomposition of alkoxy radicals.[41]

[f] This value should be considered as a low value for the rate coefficient of sulfate radical anion ($SO_4^{\bullet-}$) and organic molecules in aqueous phase.

[g] This value is treated as a low value for the pseudo-first order rate constant for the reaction between sulfate radical anion ($SO_4^{\bullet-}$) and water in the particle phase.

[h] The value refers to the equilibrium constant for bisulfate ion and sulfate ion at a given acidity.

RESULTS AND DISCUSSION

Chromatograms of Sodium Methyl Sulfate

Figure 2 shows the chromatograms of CH_3SO_4Na before and after heterogenous OH oxidation. Before oxidation (Figure 2a), the major peak corresponds to $CH_3SO_4^-$. The small peak representing SO_4^{2-} is likely originated from CH_3SO_4Na (~ 3 %) in accord with that observed in CH_3SO_4Na standard (SI Figure S1). After oxidation, the intensity of $CH_3SO_4^-$ decreases, while the intensity of SO_4^{2-} increases (Figure 2b). The detection of SO_4^{2-} supports the proposed reaction mechanisms (Scheme 1) that HSO_4^- and SO_4^{2-} are formed upon heterogeneous OH oxidation.[23] At a given OH exposure, the amount of methyl sulfate ions and sulfate ions is proportional to their peak areas in the chromatogram. The concentration of the species is then determined using the standard calibration curves (SI, Figure S2). Based on the concentrations of $CH_3SO_4^-$ and SO_4^{2-} measured at different OH exposures, we quantify the oxidation kinetics by measuring the decay of CH_3SO_4Na and determine the significance of inorganic sulfur formation.

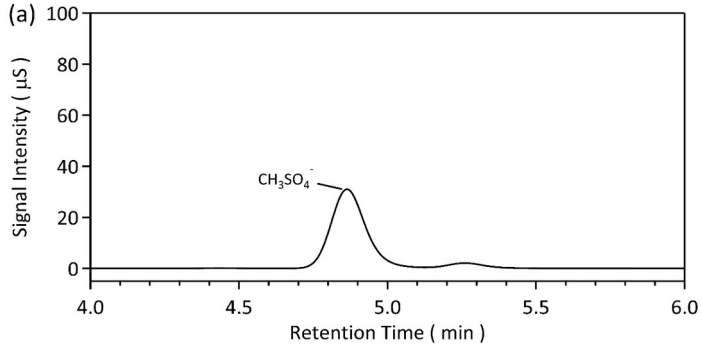

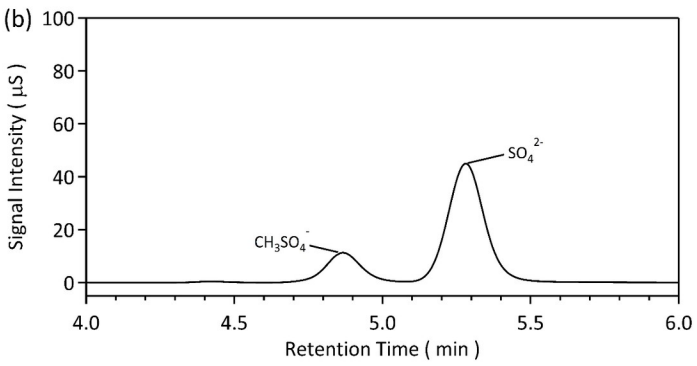

Figure 2. The chromatograms of sodium methyl sulfate (CH_3SO_4Na): (a) before oxidation; (b) after oxidation (OH exposure = 19.0×10^{11} molecules cm^{-3} s).

Oxidation Kinetics

The oxidation kinetics can be determined by the change in the concentration of $CH_3SO_4^-$ measured at different OH exposures. An effective heterogeneous OH oxidation rate constant, k, can be fitted using the exponential equation:[47]

$$\ln \frac{I}{I_0} = -k[OH] \cdot t \quad (3)$$

where I is the concentration of $CH_3SO_4^-$ after oxidation, I_0 is the concentration of $CH_3SO_4^-$ before oxidation, and $[OH]$·t refers to the OH exposure. Figure 3 shows the normalized decay of $CH_3SO_4^-$ as a function of OH exposure. The k value is fitted to be $(5.72 \pm 0.14) \times 10^{-13}$ cm^3 $molecule^{-1}$ s^{-1}. An effective OH uptake coefficient, γ_{eff}, defined as the fraction of OH collision that leads to a reaction, can be also computed with the k value:[48]

$$\gamma_{\text{eff}} = \frac{2\,k\,D_0\,\rho_p\,\text{mfs}\,N_A}{3\,M_w\,c'_{OH}} \quad (4)$$

where D_0 is the surface-weighted particle diameter obtained from the SMPS before oxidation (D_0 = 204 nm, Table 1), ρ_p is the particle density, *mfs* is the mass fraction of solute (i.e. methyl sulfate), N_A is Avogadro's constant, M_w is the molecular weight of CH_3SO_4Na, and c'_{OH} is the

average speed of gas-phase OH radical. The *mfs* can be estimated using the growth factor, G_f, of CH_3SO_4Na particles measured at a given RH, *i*:[24]

$$G_{f,\mathrm{i}} = \left(\frac{\mathrm{mfs}_{\mathrm{ref}}}{\mathrm{mfs}_{\mathrm{i}}} \frac{\rho_{\mathrm{p,ref}}}{\rho_{\mathrm{p,i}}} \right)^{\frac{1}{3}} \quad (5)$$

where mfs_{ref} and $\rho_{p,ref}$ are the mass fraction of solute and particle density at a reference RH (RH < 10 %). By assuming that CH_3SO_4Na particles are anhydrous at the reference RH[23] and using the volume additivity rule for estimating the particle density,[49] the *mfs* can be calculated as follows:

$$\mathrm{mfs}_{\mathrm{i}} = \left(1 + \frac{\rho_w}{\rho_s} \left({G_{f,\mathrm{i}}}^3 - 1 \right) \right)^{-1} \quad (6)$$

where ρ_s and ρ_w are the density of CH_3SO_4Na (1.60 g cm^{-3}) and water, respectively. At 75 % RH, the *mfs* of CH_3SO_4Na is estimated to be 0.458. Using the particle composition and size data, the γ_{eff} is calculated to be 0.31 ± 0.06. It is noted that the γ_{eff} measured at a lower RH (75 % RH) in this work is larger than that reported in our previous study carried out at a higher RH (γ_{eff} = 0.17 ± 0.03 at 85 % RH).[23] These results suggest that the RH might play a role in determining the heterogeneous reactivity. One likely explanation is that when the RH increases, CH_3SO_4Na particles absorb more water and become more diluted. For instance, from the hygroscopic data, the *mfs* decreases from 0.458 to 0.359 (~ 22 %) when the RH increases from 75 % to 85 %.[24] The surface concentration of CH_3SO_4Na is lower at higher RH. This decreases the reactive collision probability between CH_3SO_4Na and gas-phase OH radical at the particle surface, reducing the overall reaction rate (i.e. a smaller γ_{eff}).[48, 50]

Recently, molecular dynamic simulations show that the heterogeneous reaction is likely not initiated by the direct collision between a gas-phase OH radical and an organic molecule (e.g. erythritol) present at the particle surface.[51] Gas-phase OH radical is first absorbed by the particle, and an absorbed OH radical would need to collide with an organic molecule many times by

diffusion before the reaction could happen. At a higher RH, the particle contains more water, lowering the concentrations of organic molecules and adsorbed OH radical. This would make the average distance between the OH radical and its nearest organic molecules longer, slowing down the overall rate of the reaction.[51] This is consistent with a slower heterogeneous reactivity observed at a higher RH. The effect of RH and aerosol water content on the heterogeneous kinetics will be examined using a kinetic model.

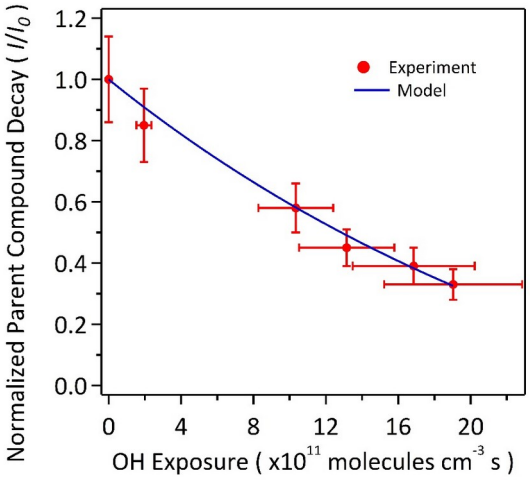

Figure 3. Normalized decay of sodium methyl sulfate (CH_3SO_4Na) as a function of OH exposure at 75 % RH.

Using the kinetic data obtained in this work and reported in the literature, we also estimate the e-folding lifetime (τ) of CH_3SO_4Na against heterogeneous OH oxidation ($\tau = 1/ (k \cdot [OH]_{ambient})$). The τ is calculated to be 13.5 ± 0.34 days at 75 % RH and 20.4 ± 1.07 days at 85 % RH, assuming an average ambient gas-phase OH concentration, $[OH]_{ambient}$, of 1.5×10^6 molecules cm^{-3}.[52] Considering atmospheric fine particles with a similar size (~200 nm) having a typical lifetime of 10 – 14 days,[53] the heterogeneous OH oxidation could be a competitive sink for CH_3SO_4Na under humid conditions. These results might also suggest that the abundance of

CH_3SO_4Na reported in the literature could be underestimated if removal processes have not been properly accounted for in field and modelling studies. It would be imperative to obtain better understanding of the transformation of CH_3SO_4Na and other organosulfates as well through heterogeneous oxidation and other atmospheric processes such as hydrolysis.

Formation of Inorganic Sulfur Species during Oxidation

To investigate the significance of inorganic sulfur formation upon oxidation, we determine the molar yield, which is defined as the total number of moles of HSO_4^- and SO_4^{2-} (i.e. $[SO_4^{2-}]$ quantified by the IC) formed per mole of CH_3SO_4Na reacted as a function of OH exposure, and computed as follows:

$$Molar\ Yield = \Delta ¿ ¿ \quad (7)$$

As shown in Figure 4, a significant amount of HSO_4^- and SO_4^{2-} is produced upon oxidation. The molar yield ranges from 0.54 ± 0.48 to 0.74 ± 0.15 when OH exposure increases from 2.0×10^{11} to 19.0×10^{11} molecules cm^{-3} s. The large uncertainty observed at the lowest OH exposure is attributed to relatively large experimental error when the change in $CH_3SO_4^-$ and SO_4^{2-} concentrations are small during oxidation (See the SI for the details on determining uncertainties of molar yield). An average yield of 0.62 ± 0.18 suggests that there is a significant conversion of organic sulfur to inorganic sulfur upon oxidation. The yields smaller than one indicates that HSO_4^- and SO_4^{2-} are likely not the only inorganic sulfur species produced upon OH oxidation of CH_3SO_4Na. For instance, at the maximum OH exposure, about 20 % of the total particle sulfur cannot be accounted by the unreacted CH_3SO_4Na, HSO_4^- and SO_4^{2-} (Figure 5a). As proposed in Scheme 1, CH_3SO_4Na tends to fragment into a formaldehyde and a $SO_4^{\bullet-}$ upon oxidation. $SO_4^{\bullet-}$ can abstract a hydrogen atom from a neighboring molecule (i.e. CH_3SO_4Na) to form HSO_4^-

(Table 2, **R6**), which exists in an equilibrium with SO_4^{2-} (Table 2, **R9**). In addition to HSO_4^- and SO_4^{2-}, $S_2O_8^{2-}$ can be formed through the self-reaction of two $SO_4^{\bullet-}$ (Table 2, **R7**). In our previous study,[23] a small SO_4^- peak has been observed in the particle-DART mass spectra and is likely attributed to the formation of $S_2O_8^{2-}$ based on its charge-to-mass ratio. Since the ionization efficiency of $S_2O_8^{2-}$ is not known in the particle-DART analysis, $S_2O_8^{2-}$ concentration cannot be determined. In this work, we have run the sodium peroxydisulfate ($Na_2S_2O_8$) standard using the IC method described in previous section in an attempt to quantify $S_2O_8^{2-}$ formed upon oxidation. However, a peak corresponding to $S_2O_8^{2-}$ was not observed in the chromatogram. This can be explained by that $S_2O_8^{2-}$ is a strongly retained ion due to its large size and its high negative charge,[54] thus eluding detection by IC. Although we were unable to confirm the presence of $S_2O_8^{2-}$ by our IC method, we postulate that $S_2O_8^{2-}$ is likely produced upon oxidation based on proposed reaction pathways (Scheme 1) and $SO_4^{\bullet-}$ chemistry reported in the literature. Future investigation on the quantification of $S_2O_8^{2-}$ upon OH oxidation of CH_3SO_4Na and other organosulfates is desirable.

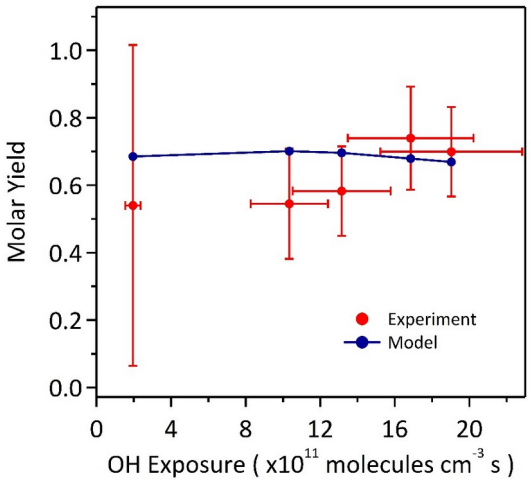

Figure 4. Molar yield of inorganic sulfur species (HSO_4^- and SO_4^{2-}) as a function of OH exposure during heterogeneous OH oxidation of sodium methyl sulfate (CH_3SO_4Na) particles at 75 % RH.

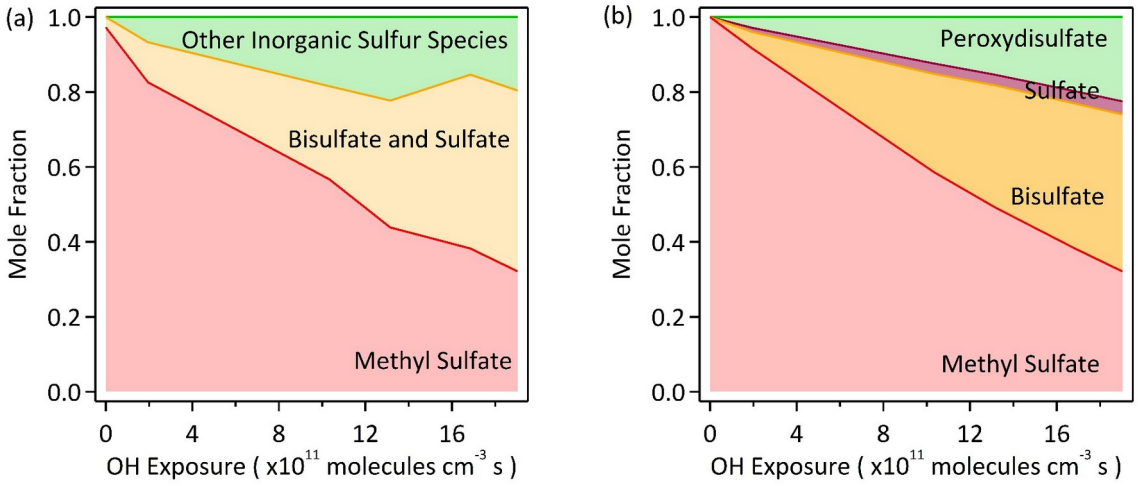

Figure 5. (a) The molar contribution of methyl sulfate ($CH_3SO_4^-$), bisulfate (HSO_4^-) and sulfate (SO_4^{2-}) , and unquantified inorganic sulfur species to total particle sulfur as a function of OH exposure during heterogeneous OH oxidation of sodium methyl sulfate (CH_3SO_4Na) at 75 % RH. (b) The molar contribution of methyl sulfate, bisulfate, sulfate and peroxydisulfate ($S_2O_8^{2-}$) to total particle sulfur predicted by the kinetic model at different OH exposures.

Kinetic Model

Figures 3 and 4 show the oxidation kinetics and concentration of inorganic sulfur species (HSO_4^- and SO_4^{2-}) predicted by the model compare well with the measurements. For example, the effective heterogenous OH rate constant, k is predicted to be $5.69 \pm 0.15 \times 10^{-13}$ cm^3 $molecule^{-1}$ s^{-1} (Table S2), which agrees well with the experimental one ($5.72 \pm 0.14 \times 10^{-13}$ cm^3 $molecule^{-1}$ s^{-1}). The average molar yield (0.69) predicted by the model is in a good agreement

with the measured one (~ 0.62). Although the model can reasonably reproduce the measurements, there are uncertainties in the rate constants. Sensitivity of the model performance towards the reactions is examined by varying the rate constants (SI, Figure S4). Upon oxidation, gas-phase OH radical is first adsorbed onto the surface of the particles. In the sensitivity test, assuming ± 100 % variation in the suggested k_{ads} value, the kinetics (i.e. k) was found to change significantly. For instance, the k was increased by about a factor of 2 when the k_{ads} was increased by 100 %. These results may not be surprising because when the k_{ads} was increased, the concentration of adsorbed OH radicals also increased, leading to a higher oxidation rate. On the other hand, the simulated composition of the inorganic sulfur species (e.g. molar yield) did not largely depend on the k_{ads}. This could be explained by that the formation of inorganic sulfur species is primarily governed by the competitions between various $SO_4^{\bullet-}$ reactions (Table 2, **R6** to **R8**).

As shown **Scheme 1**, OH radical can initiate the oxidation by abstracting a hydrogen atom from CH_3SO_4Na to form a water molecule, creating an alkyl radical, which will react with an oxygen molecule to form a peroxyl radical at rate that is known to be fast. The alkoxy radicals resulted from the self-reactions of two peroxyl radicals are expected to dissociate. In the sensitivity test, assuming ± 100 % variation in the rate constants of the reactions among these radicals (Table 2, **R1** to **R4**), we have found deviations in the simulated concentration of CH_3SO_4Na are less 0.5 %, except **R4**. These results show the model is not particularly sensitive to how the values for **R1** to **R3** are set and the suggested rate constants might be good enough to use without causing significant errors. On the other hand, the simulated kinetics and the composition of the particles were found to depend on the dissociation rate of alkoxy radicals (**R4**). For instance, when the

rate constant of **R4** was increased by 100 % of its suggested value, both the kinetics (i.e. k) and the molar yield were found to decrease by 39.2 % and 16.5 %, respectively. This could be explained by that when the dissociation rate of alkoxy radicals (**R4)** was increased, the formation rate of $SO_4^{\bullet-}$ was also increased, enhancing the self-reactions of $SO_4^{\bullet-}$ (**R7**) and slowing down the reactions of $SO_4^{\bullet-}$ with CH_3SO_4Na (**R6**) and water (**R8**). This would reduce the formation of HSO_4^- (i.e. molar yield) and secondary chain reactions (i.e. the overall reaction rate) via **R6**.

The $SO_4^{\bullet-}$, resulted from the decomposition of CH_3SO_4Na, can react with various species (e.g. CH_3SO_4Na, H_2O and $SO_4^{\bullet-}$) within the particle, governing the heterogeneous kinetics and the formation of reaction products (Table 2, **R6** to **R8**). The rate constants for these reactions are examined in sensitivity tests. When the rate constants are varied by ± 100 % of their suggested values according to Table 2, there is no significant effect on the calculated concentrations except for the reaction of $SO_4^{\bullet-}$ with CH_3SO_4Na (Table 2, **R6**). For instance, for the $SO_4^{\bullet-}$ reactions with $SO_4^{\bullet-}$ (Table 2, **R7**) or H_2O (Table 2, **R8**), when their rate constants were increased or decreased to 2 times of their suggested values, there was only minor effect on the calculated concentrations (SI, Figure S4). The variation was observed with a maximum difference of 3.5 % in CH_3SO_4Na concentration when rate constant for **R7** was increased. On the other hand, for the reaction of $SO_4^{\bullet-}$ with CH_3SO_4Na (**R6**), when the rate was increased by 100 %, the concentration of CH_3SO_4Na was decreased significantly by 66.7 % at the maximum OH exposure. As can be seen in the Figure S4 (SI), the model predicts a much faster consumption of CH_3SO_4Na (k = 1.06 × 10^{-12} cm^3 $molecule^{-1}$ s^{-1}). These results also suggest that the decay of CH_3SO_4Na upon oxidation is due to OH as well as $SO_4^{\bullet-}$ reactions. Furthermore, the rate of conversion of $SO_4^{\bullet-}$ into HSO_4^- is increased through this reaction. A higher sulfur molar yield (0.77) is also predicted (SI, Figure

S4). We would also like to note that the variation of evaporation rate of the formaldehyde (**R5**) did not influence the simulated results (SI, Figure S4).

As shown in reaction mechanisms (Scheme 1), HSO_4^- and SO_4^{2-} can be formed upon heterogeneous OH oxidation. The IC method used in this work does not allow to individually determine the relative abundance of HSO_4^-, SO_4^{2-} and $S_2O_8^{2-}$. Model simulations show that the amount of inorganic sulfur species formed upon oxidation is mostly dominated by HSO_4^-, followed by $S_2O_8^{2-}$ and SO_4^{2-}. We acknowledge that $S_2O_8^{2-}$ formed through the self-reactions of two $SO_4^{\bullet-}$ would account for the remaining inorganic sulfur species in the model. Overall, the results of sensitivity tests have identified a few reaction setups (the OH adsorption rate (k_{ads}), dissociation rate of alkoxy radicals (**R4**) and reaction rate of $SO_4^{\bullet-}$ with CH_3SO_4Na (**R6**)) could have the significant influence on the calculated kinetics and inorganic sulfur species concentrations. Thus, priority on these reactions are suggested for future studies.

We also used the model to examine the effect of RH and aerosol water content on the heterogeneous kinetics. In model simulations, when the RH increases from 75 % to 85 %, the initial concentration of CH_3SO_4Na decreases based on the hygroscopic data.[24] As shown in Figure S5 (SI), the model can well predict the kinetic data reported in the literature,[23] supporting the hypothesis that a decrease in the surface concentration of CH_3SO_4Na at a higher RH could lower the overall rate of reactions between CH_3SO_4Na and OH radical at the particle surface through dilution.[48, 50] Additionally, the model predicts an average molar yield of ~ 0.64 which is not very sensitive to the variation in RH (SI, Figure S6).

CONCLUSIONS

In this work, we show that a significant amount of inorganic sulfur species can be produced during heterogenous OH oxidation of CH_3SO_4Na at an efficient rate. The molar yield of HSO_4^- and SO_4^{2-} is significant. Inorganic sulfur species (e.g. $S_2O_8^{2-}$) other than HSO_4^- and SO_4^{2-} is likely formed through the particle-phase reactions initiated by $SO_4^{\bullet-}$, which cannot be quantified by the IC method used in our study. Further studies on sulfur balance (i.e. both inorganic and organic sulfur species) upon heterogeneous OH oxidation of CH_3SO_4Na and other organosulfates are highly desirable to better understand how the form of sulfur would change during oxidation.

A kinetic model has been developed that describes the reaction kinetics and products of CH_3SO_4Na particles upon oxidation. The results of sensitivity tests have identified a few reaction steps such as the OH adsorption, dissociation of alkoxy radicals (**R4**) and reaction of $SO_4^{\bullet-}$ with CH_3SO_4Na (**R6**) could have the significant influence on the calculated kinetics and inorganic sulfur species concentrations. The modeled results also support the hypothesis that the decrease in heterogeneous kinetics (i.e. γ_{eff}) observed at higher RH could be explained by the dilution effect. To date, rate constants for the reactions of organosulfates and their radical intermediates with OH radical and other oxidants are virtually non-existent in the literature. The knowledge of the rates of these reactions is essential for the future model development.

More recently, the heterogenous OH oxidation of isoprene-derived organosulfates (e.g. 2-methyltetrol sulfate esters and 3-methyltetrol sulfate esters), one of the most abundant organosulfates detected in atmospheric particles, can lead to the formation of HSO_4^-.[55-56] Further studies are needed to study the significance of the formation of inorganic sulfur species upon heterogeneous OH oxidation of organosulfates. In this work, we have demonstrated that IC method can be used to quantify the amount of inorganic sulfates (a total sum of HSO_4^- and

SO_4^{2-}) formed upon oxidation. Since inorganic sulfur species other than HSO_4^- and SO_4^{2-} can be formed upon oxidation of organosulfates, the detection and quantification of inorganic sulfur species, including $S_2O_8^{2-}$ is desirable, especially in laboratory studies for particle sulfur balance. Overall, a better knowledge of the kinetics and chemistry of $SO_4^{\bullet-}$ chemistry would allow us to better understand and predict the transformation of organosulfates to inorganic sulfur species through heterogeneous OH oxidation and other atmospheric processes such as hydrolysis and aqueous-phase oxidation, and the associated impacts of such reactions on atmospheric particle sulfur cycle.

Acknowledgements: K.C.K., R.X., H.Y.P. and M.N.C. are supported by the Hong Kong Research Grants Council (HKRGC): Project ID 2130626 (Ref 14300118). K.R.W. is supported by the Condensed Phase and Interfacial Molecular Science Program (CPIMS), in the Chemical Sciences Geosciences and Biosciences Division of the Office of Basic Energy Sciences of the U.S. Department of Energy under Contract No. DE-AC02-05CH11231.

Supporting Information Available: Additional details for uncertainty determination; ancillary figures for model simulation results.

References:

1. Surratt, J. D.; Gómez-González, Y.; Chan, A. W. H.; Vermeylen, R.; Shahgholi, M.; Kleindienst, T. E.; Edney, E. O.; Offenberg, J. H.; Lewandowski, M.; Jaoui, M.; Maenhaut, W.; Claeys, M.; Flagan, R. C.; Seinfeld, J. H. Organosulfate Formation in Biogenic Secondary Organic Aerosol. *J. Phys. Chem. A* **2008,** *112*, 8345−8378, 10.1021/jp802310p.
2. Tolocka, M. P.; Turpin, B. Contribution of Organosulfur Compounds to Organic Aerosol Mass. *Environ. Sci. Technol.* **2012,** *46*, 7978−7983, 10.1021/es300651v.
3. Brüggemann, M.; Xu, R.; Tilgner, A.; Kwong, K. C.; Mutzel, A.; Poon, H. Y.; Otto, T.; Schaefer, T.; Poulain, L.; Chan, M. N.; Herrmann, H. Organosulfates in Ambient Aerosol: State of Knowledge and Future Research Directions on Formation, Abundance, Fate, and Importance. *Environ. Sci. Technol.* **2020,** *54*, 3767−3782, 10.1021/acs.est.9b06751.

4. Iinuma, Y.; Böge, O.; Gnauk, T.; Herrmann, H. Aerosol-chamber Study of the α-pinene/O_3 Reaction: Influence of Particle Acidity on Aerosol Yields and Products. *Atmos. Environ.* **2004,** *38*, 761−773, https://doi.org/10.1016/j.atmosenv.2003.10.015.

5. Iinuma, Y.; Böge, O.; Kahnt, A.; Herrmann, H. Laboratory Chamber Studies on the Formation of Organosulfates from Reactive Uptake of Monoterpene Oxides. *Phys. Chem. Chem. Phys.* **2009,** *11*, 7985−7997, 10.1039/B904025K.

6. Iinuma, Y.; Müller, C.; Berndt, T.; Böge, O.; Claeys, M.; Herrmann, H. Evidence for the Existence of Organosulfates from β-Pinene Ozonolysis in Ambient Secondary Organic Aerosol. *Environ. Sci. Technol.* **2007,** *41*, 6678−6683, 10.1021/es070938t.

7. Iinuma, Y.; Müller, C.; Böge, O.; Gnauk, T.; Herrmann, H. The Formation of Organic Sulfate Esters in the Limonene Ozonolysis Secondary Organic Aerosol (SOA) under Acidic Conditions. *Atmos. Environ.* **2007,** *41*, 5571−5583, https://doi.org/10.1016/j.atmosenv.2007.03.007.

8. Liggio, J.; Li, S.-M. Organosulfate Formation during the Uptake of Pinonaldehyde on Acidic Sulfate Aerosols. *Geophys. Res. Lett.* **2006,** *33*, L13808, 10.1029/2006GL026079.

9. Liggio, J.; Li, S.-M. Reactive Uptake of Pinonaldehyde on Acidic Aerosols. *J. Geophys. Res.: Atmos.* **2006,** *111*, D24303, 10.1029/2005JD006978.

10. Liggio, J.; Li, S.-M.; McLaren, R. Heterogeneous Reactions of Glyoxal on Particulate Matter: Identification of Acetals and Sulfate Esters. *Environ. Sci. Technol.* **2005,** *39*, 1532−1541, 10.1021/es048375y.

11. Ma, Y.; Xu, X.; Song, W.; Geng, F.; Wang, L. Seasonal and Diurnal Variations of Particulate Organosulfates in Urban Shanghai, China. *Atmos. Environ.* **2014,** *85*, 152−160, https://doi.org/10.1016/j.atmosenv.2013.12.017.

12. McNeill, V. F.; Woo, J. L.; Kim, D. D.; Schwier, A. N.; Wannell, N. J.; Sumner, A. J.; Barakat, J. M. Aqueous-phase Secondary Organic Aerosol and Organosulfate Formation in Atmospheric Aerosols: A Modeling Study. *Environ. Sci. Technol.* **2012,** *46*, 8075−8081, 10.1021/es3002986.

13. Minerath, E. C.; Elrod, M. J. Assessing the Potential for Diol and Hydroxy Sulfate Ester Formation from the Reaction of Epoxides in Tropospheric Aerosols. *Environ. Sci. Technol.* **2009,** *43*, 1386−1392, 10.1021/es8029076.

14. Nozière, B.; Ekström, S.; Alsberg, T.; Holmström, S. Radical-initiated Formation of Organosulfates and Surfactants in Atmospheric Aerosols. *Geophys. Res. Lett.* **2010,** *37*, L05806, 10.1029/2009GL041683.

15. Riva, M.; Da Silva Barbosa, T.; Lin, Y. H.; Stone, E. A.; Gold, A.; Surratt, J. D. Chemical Characterization of Organosulfates in Secondary Organic Aerosol Derived from the Photooxidation of Alkanes. *Atmos. Chem. Phys.* **2016,** *16*, 11001−11018, 10.5194/acp-16-11001-2016.

16. Rudziński, K. J.; Gmachowski, L.; Kuznietsova, I. Reactions of Isoprene and Sulphoxy radical-anions – A Possible Source of Atmospheric Organosulphites and Organosulphates. *Atmos. Chem. Phys.* **2009,** *9*, 2129−2140, 10.5194/acp-9-2129-2009.

17. Stone, E. A.; Yang, L.; Yu, L. E.; Rupakheti, M. Characterization of Organosulfates in Atmospheric Aerosols at Four Asian Locations. *Atmos. Environ.* **2012,** *47*, 323−329, https://doi.org/10.1016/j.atmosenv.2011.10.058.

18. Surratt, J. D.; Chan, A. W. H.; Eddingsaas, N. C.; Chan, M.; Loza, C. L.; Kwan, A. J.; Hersey, S. P.; Flagan, R. C.; Wennberg, P. O.; Seinfeld, J. H. Reactive Intermediates Revealed in Secondary Organic Aerosol Formation from Isoprene. *Proc. Natl. Acad. Sci.* **2010,** *107*, 6640−6645, 10.1073/pnas.0911114107.
19. Surratt, J. D.; Kroll, J. H.; Kleindienst, T. E.; Edney, E. O.; Claeys, M.; Sorooshian, A.; Ng, N. L.; Offenberg, J. H.; Lewandowski, M.; Jaoui, M.; Flagan, R. C.; Seinfeld, J. H. Evidence for Organosulfates in Secondary Organic Aerosol. *Environ. Sci. Technol.* **2007,** *41*, 517−527, 10.1021/es062081q.
20. Wach, P.; Spólnik, G.; Rudziński, K. J.; Skotak, K.; Claeys, M.; Danikiewicz, W.; Szmigielski, R. Radical Oxidation of Methyl Vinyl Ketone and Methacrolein in Aqueous Droplets: Characterization of Organosulfates and Atmospheric Implications. *Chemosphere* **2019,** *214*, 1−9, https://doi.org/10.1016/j.chemosphere.2018.09.026.
21. Wang, Y.; Hu, M.; Guo, S.; Wang, Y.; Zheng, J.; Yang, Y.; Zhu, W.; Tang, R.; Li, X.; Liu, Y.; Le Breton, M.; Du, Z.; Shang, D.; Wu, Y.; Wu, Z.; Song, Y.; Lou, S.; Hallquist, M.; Yu, J. The Secondary Formation of Organosulfates under Interactions between Biogenic Emissions and Anthropogenic Pollutants in Summer in Beijing. *Atmos. Chem. Phys.* **2018,** *18*, 10693−10713, 10.5194/acp-18-10693-2018.
22. Hu, K. S.; Darer, A. I.; Elrod, M. J. Thermodynamics and Kinetics of the Hydrolysis of Atmospherically Relevant Organonitrates and Organosulfates. *Atmos. Chem. Phys.* **2011,** *11*, 8307−8320, 10.5194/acp-11-8307-2011.
23. Kwong, K. C.; Chim, M. M.; Davies, J. F.; Wilson, K. R.; Chan, M. N. Importance of Sulfate Radical Anion Formation and Chemistry in Heterogeneous OH Oxidation of Sodium Methyl Sulfate, the Smallest Organosulfate. *Atmos. Chem. Phys.* **2018,** *18*, 2809−2820, 10.5194/acp-18-2809-2018.
24. Estillore, A. D.; Hettiyadura, A. P. S.; Qin, Z.; Leckrone, E.; Wombacher, B.; Humphry, T.; Stone, E. A.; Grassian, V. H. Water Uptake and Hygroscopic Growth of Organosulfate Aerosol. *Environ. Sci. Technol.* **2016,** *50*, 4259−4268, 10.1021/acs.est.5b05014.
25. Hansen, A. M. K.; Hong, J.; Raatikainen, T.; Kristensen, K.; Ylisirniö, A.; Virtanen, A.; Petäjä, T.; Glasius, M.; Prisle, N. L. Hygroscopic Properties and Cloud Condensation Nuclei Activation of Limonene-derived Organosulfates and their Mixtures with Ammonium Sulfate. *Atmos. Chem. Phys.* **2015,** *15*, 14071−14089, 10.5194/acp-15-14071-2015.
26. Hyttinen, N.; Elm, J.; Malila, J.; Calderón, S. M.; Prisle, N. L. Thermodynamic Properties of Isoprene- and Monoterpene-derived Organosulfates Estimated with COSMOtherm. *Atmos. Chem. Phys.* **2020,** *20*, 5679−5696, 10.5194/acp-20-5679-2020.
27. Mitroo, D.; Sun, Y.; Combest, D. P.; Kumar, P.; Williams, B. J. Assessing the Degree of Plug Flow in Oxidation Flow Reactors (OFRs): A Study on A Potential Aerosol Mass (PAM) Reactor. *Atmos. Meas. Tech.* **2018,** *11*, 1741−1756, 10.5194/amt-11-1741-2018.
28. Kang, E.; Root, M. J.; Toohey, D. W.; Brune, W. H. Introducing the Concept of Potential Aerosol Mass (PAM). *Atmos. Chem. Phys.* **2007,** *7*, 5727−5744, 10.5194/acp-7-5727-2007.
29. Lambe, A. T.; Ahern, A. T.; Williams, L. R.; Slowik, J. G.; Wong, J. P. S.; Abbatt, J. P. D.; Brune, W. H.; Ng, N. L.; Wright, J. P.; Croasdale, D. R.; Worsnop, D. R.; Davidovits, P.; Onasch, T. B. Characterization of Aerosol Photooxidation Flow Reactors: Heterogeneous Oxidation, Secondary Organic Aerosol Formation and Cloud Condensation Nuclei Activity Measurements. *Atmos. Meas. Tech.* **2011,** *4*, 445−461, 10.5194/amt-4-445-2011.

30. Liu, T.; Li, Z.; Chan, M.; Chan, C. K. Formation of Secondary Organic Aerosols from Gas-phase Emissions of Heated Cooking Oils. *Atmos. Chem. Phys.* **2017,** *17*, 7333–7344, 10.5194/acp-17-7333-2017.
31. Huang, X. H. H.; Bian, Q.; Ng, W. M.; Louie, P. K. K.; Yu, J. Z. Characterization of PM2.5 Major Components and Source Investigation in Suburban Hong Kong: A One Year Monitoring Study. *Aerosol Air Qual. Res.* **2014,** *14*, 237–250, 10.4209/aaqr.2013.01.0020.
32. Liu, M. J.; Wiegel, A. A.; Wilson, K. R.; Houle, F. A. Aerosol Fragmentation Driven by Coupling of Acid–Base and Free-Radical Chemistry in the Heterogeneous Oxidation of Aqueous Citric Acid by OH Radicals. *J. Phys. Chem. A* **2017,** *121*, 5856–5870, 10.1021/acs.jpca.7b04892.
33. Richards-Henderson, N. K.; Goldstein, A. H.; Wilson, K. R. Large Enhancement in the Heterogeneous Oxidation Rate of Organic Aerosols by Hydroxyl Radicals in the Presence of Nitric Oxide. *J. Phys. Chem. Lett.* **2015,** *6*, 4451–4455, 10.1021/acs.jpclett.5b02121.
34. Richards-Henderson, N. K.; Goldstein, A. H.; Wilson, K. R. Sulfur Dioxide Accelerates the Heterogeneous Oxidation Rate of Organic Aerosol by Hydroxyl Radicals. *Environ. Sci. Technol.* **2016,** *50*, 3554–3561, 10.1021/acs.est.5b05369.
35. Heine, N.; Houle, F. A.; Wilson, K. R. Connecting the Elementary Reaction Pathways of Criegee Intermediates to the Chemical Erosion of Squalene Interfaces during Ozonolysis. *Environ. Sci. Technol.* **2017,** *51*, 13740–13748, 10.1021/acs.est.7b04197.
36. Houle, F. A.; Hinsberg, W. D.; Wilson, K. R. Oxidation of A Model Alkane Aerosol by OH Radical: the Emergent Nature of Reactive Uptake. *Phys. Chem. Chem. Phys.* **2015,** *17*, 4412–4423, 10.1039/C4CP05093B.
37. Wiegel, A. A.; Wilson, K. R.; Hinsberg, W. D.; Houle, F. A. Stochastic Methods for Aerosol Chemistry: A Compact Molecular Description of Functionalization And Fragmentation in the Heterogeneous Oxidation of Squalane Aerosol by OH Radicals. *Phys. Chem. Chem. Phys.* **2015,** *17*, 4398–4411, 10.1039/C4CP04927F.
38. Monod, A.; Doussin, J. F. Structure-Activity Relationship for the Estimation of OH-Oxidation Rate Constants of Aliphatic Organic Compounds in the Aqueous Phase: Alkanes, Alcohols, Organic Acids and Bases. *Atmos. Environ.* **2008,** *42*, 7611–7622, https://doi.org/10.1016/j.atmosenv.2008.06.005.
39. Marchaj, A.; Kelley, D. G.; Bakac, A.; Espenson, J. H. Kinetics of the Reactions between Alkyl Radicals and Molecular Oxygen in Aqueous Solution. *J. Phys. Chem.* **1991**. *95*, 4440–4441, doi:10.1021/j100164a051.
40. Nikolaev, A. I. S., R. L.; Enikeeva, L. R.; Komissarov, V. D. Decay Kinetics of Methylperoxy Radicals in Liquid Phase. *Khim. Fizika.* **1992,** *11*, 69–72.
41. Vereecken, L.; Peeters, J. Decomposition of Substituted Alkoxy Radicals—Part I: A Generalized Structure–Activity Relationship for Reaction Barrier Heights. *Phys. Chem. Chem. Phys.* **2009,** *11*, 9062–9074, 10.1039/B909712K.
42. Huie, R. E.; Clifton, C. L. Rate Constants for Hydrogen Abstraction Reactions of the Sulfate Radical, $SO_4^{\bullet-}$ Alkanes and Ethers. *Int. J. Chem. Kinet.* **1989,** *21*, 611–619, 10.1002/kin.550210802.
43. Jiang, P.-Y.; Katsumura, Y.; Nagaishi, R.; Domae, M.; Ishikawa, K.; Ishigure, K.; Yoshida, Y. Pulse Radiolysis Study of Concentrated Sulfuric Acid Solutions. Formation Mechanism, Yield and Reactivity of Sulfate Radicals. *J. Chem. Soc., Faraday Trans.* **1992,** *88*, 1653–1658, 10.1039/FT9928801653.

44. Hayon, E.; Treinin, A.; Wilf, J. Electronic Spectra, Photochemistry, and Autoxidation Mechanism of the Sulfite-Bisulfite-Pyrosulfite Systems. SO_2^-, SO_3^-, SO_4^-, and SO_5^- radicals. *J. Chem. Soc.* **1972,** *94*, 47−57, 10.1021/ja00756a009.
45. Smith, R. M.; Martell, A. E. Critical Stability Constants, Enthalpies and Entropies for The Formation of Metal Complexes of Aminopolycarboxylic Acids and Carboxylic Acids. *Sci. Total Environ.* **1987,** *64*, 125−147, https://doi.org/10.1016/0048-9697(87)90127-6.
46. Cooper, P. L.; Abbatt, J. P. D. Heterogeneous Interactions of OH and HO_2 Radicals with Surfaces Characteristic of Atmospheric Particulate Matter. *J. Phys. Chem.* **1996,** *100*, 2249−2254, 10.1021/jp952142z.
47. Smith, J. D.; Kroll, J. H.; Cappa, C. D.; Che, D. L.; Liu, C. L.; Ahmed, M.; Leone, S. R.; Worsnop, D. R.; Wilson, K. R. The Heterogeneous Reaction of Hydroxyl Radicals with Sub-Micron Squalane Particles: A Model System for Understanding the Oxidative Aging of Ambient Aerosols. *Atmos. Chem. Phys.* **2009,** *9*, 3209−3222, 10.5194/acp-9-3209-2009.
48. Davies, J. F.; Wilson, K. R. Nanoscale Interfacial Gradients Formed by the Reactive Uptake of OH Radicals onto Viscous Aerosol Surfaces. *Chem. Sci.* **2015,** *6*, 7020−7027, 10.1039/C5SC02326B.
49. Wise, M. E.; Surratt, J. D.; Curtis, D. B.; Shilling, J. E.; Tolbert, M. A. Hygroscopic Growth of Ammonium Sulfate/Dicarboxylic Acids. *J. Geophys. Res.: Atmos.* **2003,** *108*, 4638−4646, 10.1029/2003JD003775.
50. Chim, M. M.; Lim, C. Y.; Kroll, J. H.; Chan, M. N. Evolution in the Reactivity of Citric Acid toward Heterogeneous Oxidation by Gas-Phase OH Radicals. *ACS Earth Space Chem.* **2018,** *2*, 1323−1329, 10.1021/acsearthspacechem.8b00118.
51. Xu, R.; Lam, H. K.; Wilson, K. R.; Davies, J. F.; Song, M.; Li, W.; Tse, Y. L. S.; Chan, M. N. Effect of Inorganic-to-Organic Mass Ratio on the Heterogeneous OH Reaction Rates of Erythritol: Implications for Atmospheric Chemical Stability of 2-Methyltetrols. *Atmos. Chem. Phys.* **2020,** *20*, 3879−3893, 10.5194/acp-20-3879-2020.
52. Mao, J.; Ren, X.; Brune, W. H.; Olson, J. R.; Crawford, J. H.; Fried, A.; Huey, L. G.; Cohen, R. C.; Heikes, B.; Singh, H. B.; Blake, D. R.; Sachse, G. W.; Diskin, G. S.; Hall, S. R.; Shetter, R. E. Airborne measurement of OH reactivity during INTEX-B. *Atmos. Chem. Phys.* **2009,** *9*, 163−173, , 10.5194/acp-9-163-2009.
53. Kanakidou, M.; Seinfeld, J. H.; Pandis, S. N.; Barnes, I.; Dentener, F. J.; Facchini, M. C.; Van Dingenen, R.; Ervens, B.; Nenes, A.; Nielsen, C. J.; Swietlicki, E.; Putaud, J. P.; Balkanski, Y.; Fuzzi, S.; Horth, J.; Moortgat, G. K.; Winterhalter, R.; Myhre, C. E. L.; Tsigaridis, K.; Vignati, E.; Stephanou, E. G.; Wilson, J. Organic Aerosol and Global Climate Modelling: A Review. *Atmos. Chem. Phys.* **2005,** *5*, 1053−1123, 10.5194/acp-5-1053-2005.
54. Khan, N. E.; Adewuyi, Y. G. A New Method of Analysis of Peroxydisulfate Using Ion Chromatography and Its Application to The Simultaneous Determination of Peroxydisulfate and Other Common Inorganic Ions in A Peroxydisulfate Matrix. *J. Chromatogr. A* **2011,** *1218*, 392−397, https://doi.org/10.1016/j.chroma.2010.11.038.
55. Chen, Y.; Zhang, Y.; Lambe, A. T.; Xu, R.; Lei, Z.; Olson, N. E.; Zhang, Z.; Szalkowski, T.; Cui, T.; Vizuete, W.; Gold, A.; Turpin, B. J.; Ault, A. P.; Chan, M. N.; Surratt, J. D. Heterogeneous Hydroxyl Radical Oxidation of Isoprene-Epoxydiol-Derived Methyltetrol Sulfates: Plausible Formation Mechanisms of Previously Unexplained Organosulfates in Ambient Fine Aerosols. *Environ. Sci. Technol. Letters* **2020,** *7*, 460−468, 10.1021/acs.estlett.0c00276.

56. Lam, H. K.; Kwong, K. C.; Poon, H. Y.; Davies, J. F.; Zhang, Z.; Gold, A.; Surratt, J. D.; Chan, M. N. Heterogeneous OH Oxidation of Isoprene-Epoxydiol-Derived Organosulfates: Kinetics, Chemistry and Formation of Inorganic Sulfate. *Atmos. Chem. Phys.* **2019,** *19*, 2433−2440, 10.5194/acp-19-2433-2019.

For TOC only

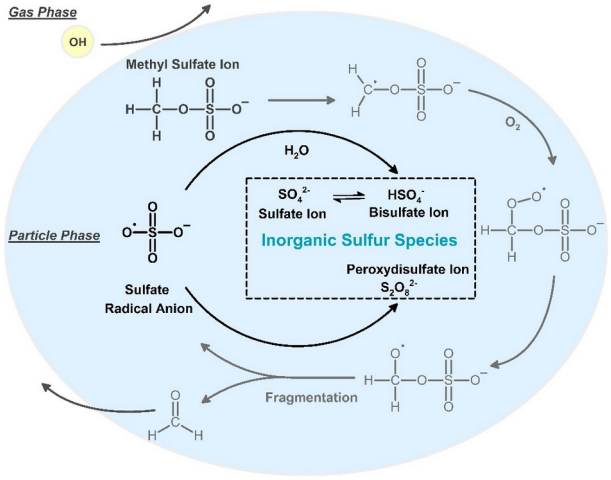
Gas Phase
OH
Methyl Sulfate Ion
H_2O
O_2
SO_4^{2-}
Sulfate Ion
HSO_4^-
Bisulfate Ion
Inorganic Sulfur Species
Peroxydisulfate Ion
$S_2O_8^{2-}$
Particle Phase
Sulfate
Radical Anion
Fragmentation